Ideal Type-II Weyl Phase and Topological Transition in Phononic Crystals

Xueqin Huang,[1] Weiyin Deng,[1,*] Feng Li,[1] Jiuyang Lu,[1,†] and Zhengyou Liu[2,3,‡]
[1]School of Physics and Optoelectronics, South China University of Technology, Guangzhou, Guangdong 510640, China
[2]Key Laboratory of Artificial Micro- and Nanostructures of Ministry of Education and School of Physics and Technology, Wuhan University, Wuhan 430072, China
[3]Institute for Advanced Studies, Wuhan University, Wuhan 430072, China

(Received 27 October 2019; accepted 1 May 2020; published 19 May 2020)

Ideal Weyl points, which are related by symmetry and thus reside at the same frequency, could offer further insight into the Weyl physics. The ideal type-I Weyl points have been observed in photonic crystals, but the ideal type-II Weyl points with tilted conelike band dispersions are still not realized. Here we present the observation of the ideal type-II Weyl points of the minimal number in three-dimensional phononic crystals and, in the meantime, the topological phase transition from the Weyl semimetal to the valley insulators of two distinct types. The Fermi-arc surface states are shown to exist on the surfaces of the Weyl phase, and the Fermi-circle surface states are also observed, but on the interface of the two distinct valley phases. Intriguing wave partition of the Fermi-circle surface states is demonstrated.

DOI: 10.1103/PhysRevLett.124.206802

Weyl semimetals, hosting twofold linear crossing points in three-dimensional (3D) momentum space, i.e., Weyl points (WPs), have stimulated intensive research in the field of topological physics [1–8]. The WP behaves as a source or sink of the Berry curvature flux and carries topological charge of $+1$ or -1 [3]. The existence of WPs needs the breaking of the spatial inversion or time-reversal symmetries. Generally, there exists at least two WPs in the system with broken time-reversal symmetry, but four in the presence of time-reversal symmetry [9]. Because of their topological nature, WPs always come in pairs, which give rise to a variety of intriguing properties, such as nonclosed Fermi-arc surface dispersions [1–3] and chiral anomaly [10–15]. In particular, WPs, described by all the three Pauli matrices, are stable against small perturbations [16]; therefore, the problem of the topological phase transition in Weyl semimetal is less explored.

There are two types of WPs: the type-I WP has a pointlike Fermi surface, while the type-II WP hosts a strongly tilted cone dispersion and possesses a conical Fermi surface [17–21]. This feature enables the type-II Weyl semimetal to exhibit numerous unique properties, including anisotropic chiral anomaly [22,23] and antichiral Landau levels [17,24]. The WPs, of both types I and II, have been achieved in condensed matter systems [25–32] and artificial periodical structures, such as photonic crystals [33–37] and phononic crystals (PCs) [38–44]. However, these WPs are usually not at the same energy, making a serious restriction for realizing and utilizing the unique properties induced by the WPs [9,45–47]. To overcome this problem, recently, the concept of ideal WPs, types I [45,46] or II [47–50], which are related by symmetry and thus reside at the same energy, has been proposed. Although the ideal type-I WPs have been achieved in photonic crystals [51], the ideal type-II Weyl phase is still beyond realization.

Benefiting from the macroscopic nature, PC is ideal for studying the topological physics and exploring the novel transport phenomena for acoustic waves. Actually, besides the Weyl phase discussed above [40–44], lots of other topological phases [52–62], including the two-dimensional valley insulator [52,53] and Chern insulator [54], have been realized in PCs. In this Letter, we realize a 3D PC, which hosts four ideal type-II WPs protected by the time-reversal and mirror symmetries. Phase transitions from the Weyl semimetal to valley insulators of two distinct phases are studied. The Fermi-arc surface states are shown to exist on the surfaces of the Weyl phase. Specifically, the Fermi-circle surface states are found on the interface of the two distinct valley phases, whose dispersions are the closed equifrequency contours [63]. A unique wave partition of the Fermi-circle surface states is demonstrated.

As shown in Fig. 1(a), the PC sample is fabricated by 3D printing. The PC is a layer-by-layer stacking of a hexagonal array of triangular scatterers, together with the supporting plate, as shown in Fig. 1(b). The plate is drilled with cutting-through holes of two different sizes, by which the neighboring layers couple. The top and side views of one unit cell are displayed in Figs. 1(c) and 1(d). The rotational angle of the triangular rod with respect to the x axis is θ. The height and side length of the triangular rod are $2h_1$ and s. The height and the radii of the coupling holes are h_2, r_1, and r_2. The lattice constants in the x-y plane and along the z direction are a and $h = 2h_1 + h_2$. The parameters are chosen as $a = \sqrt{3}$cm, $s = 0.4\sqrt{3}a$, $h_1 = 0.25a$, $h_2 = 0.1a$, $r_1 = 0.1a$, and $r_2 = 0.3r_1$. Air is filled inside the structured channels with hard boundaries marked by the cream color.

 © 2020 American Physical Society

All the simulations are performed by the COMSOL Multiphysics solver package.

To illustrate how the ideas work, we construct a tight-binding model to describe the PC. As shown in Fig. 1(e), a unit cell contains two sites (points 1 and 2), corresponding to the two inequivalent triangular-lattice centers 1 and 2 in each layer shown in Figs. 1(b) and 1(c). The site energy ε is induced by the rotational angle θ of the triangular scatterer [52,53], and the nearest-neighbor hopping t_0 is constant, denoting the intralayer coupling. The interlayer couplings t_1 and t_2 are introduced by the holes of two different sizes in the plate (r_1 and r_2), while the plate is used to separate the air and thus form the layer-by-layer stacking structure. On the basis of the sublattices 1 and 2, the Hamiltonian in momentum space can be given by

$$H = d_x\sigma_x + d_y\sigma_y + d_z\sigma_z + d_0 I, \tag{1}$$

where $d_x = t_0\cos(k_x a/\sqrt{3}) + 2t_0\cos(k_y a/2)\cos(k_x a/2\sqrt{3})$, $d_y = -t_0\sin(k_x a/\sqrt{3}) + 2t_0\cos(k_y a/2)\sin(k_x a/2\sqrt{3})$, $d_z = \varepsilon + (t_1 - t_2)\cos k_z h$, and $d_0 = (t_1 + t_2)\cos k_z h$. $\boldsymbol{\sigma}$ are the Pauli matrices represented sublattice degree of freedom, and I is the identity matrix.

The eigenvalues of the Hamiltonian (1) is $E_\pm = d_0 \pm \sqrt{d_x^2 + d_y^2 + d_z^2}$. If $t_1 = t_2$, induced by the same size of holes ($r_1 = r_2$), the equal interlayer couplings cannot result in a k_z-dependent σ_z term, thus no WP exists in this case. When $t_1 \neq t_2$ and $d_x = d_y = d_z = 0$, the band crossing occurs and forms the type-II WP with d_0 tilting the band dispersion along the k_z direction. The effective Hamiltonian near the WP is

$$\delta H_W = v_x\delta k_x\sigma_x + v_y\delta k_y\sigma_y + v_z\delta k_z\sigma_z + v_0\delta k_z I, \tag{2}$$

where $v_{i=x,y,z,0}$ are quantities related with the group velocities, and $|v_0/v_z| = |(t_1 + t_2)/(t_1 - t_2)| > 1$, verifying the WP is of type II [17]. The topological charges of WPs can be calculated as $C = \mathrm{sgn}(v_x v_y v_z) = \pm 1$, as shown in Fig. 1(f). The details of the Hamiltonian and charges of WPs are shown in the Supplemental Material [64]. On the other hand, when $d_z \neq 0$, by considering k_z as a parameter, the Hamiltonian (1) can be viewed as a two-dimensional valley insulator [65–69]. In this case, the two valleys V' and V, the frequency extrema, are located at points $(k_x, k_y) = [(2\pi/\sqrt{3}a), (2\pi/3a)]$ and $[0, (4\pi/3a)]$ for a fixed k_z. The effective Hamiltonian of valley V along the KH line [Fig. 1(f)] is derived as

$$\delta H_V = v_0\delta k_x\sigma_x + v_0\delta k_y\sigma_y + d_z\sigma_z + d_0 I, \tag{3}$$

with $v_0 = \sqrt{3}t_0 a/2$. The valley Chern number, the integral of Berry curvature near the valley [65–69], is obtained as $C_V(k_z) = \frac{1}{2}\mathrm{sgn}(d_z)$, and that of valley V' is $C_{V'}(k_z) = -C_V(k_z)$, connected by the time-reversal symmetry.

We now demonstrate the existence of the ideal type-II WPs. For the PC with $\theta = 35°$, the bulk band structure of the lowest two bands at $(k_x, k_y) = [0, (4\pi/3a)]$ along the k_z direction is calculated and measured in Fig. 1(g). The colored maps denote the experimental dispersions obtained by Fourier transforming the measured pressure fields inside the sample, while the black dashed lines represent the simulated values obtained from full-wave simulations. It is

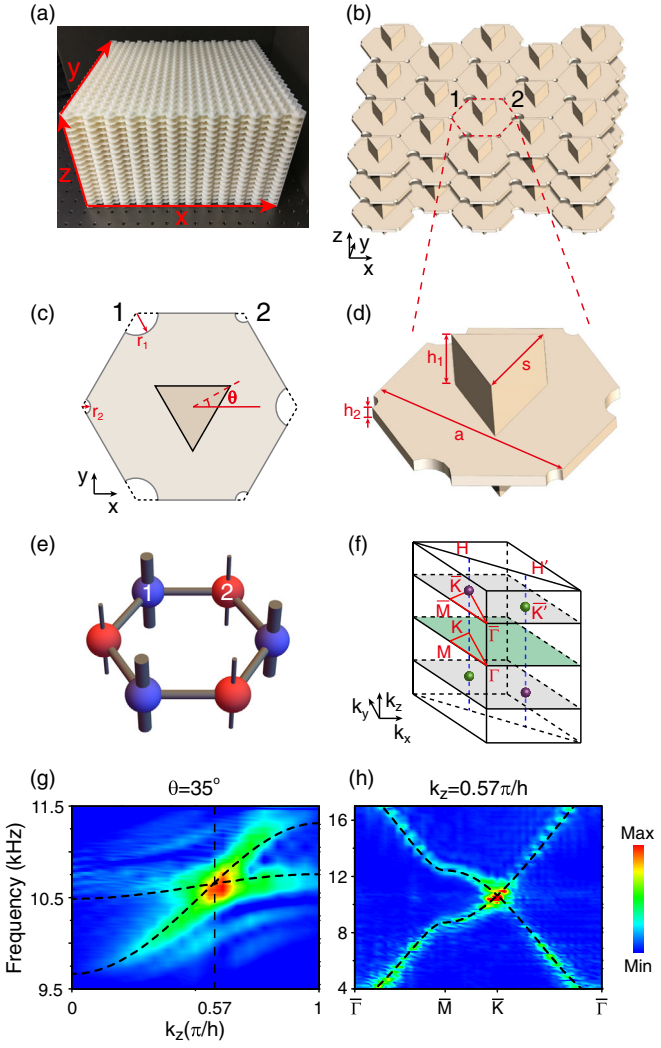

FIG. 1. (a) A photo of the 3D sample with $\theta = 35°$. (b) Schematic of the layer-by-layer stacking PC. Each layer consists of triangular rods arranged in a hexagonal lattice and couples with each other via two different sized vertical holes. The (c) top and (d) side views of the unit cell. θ is the rotation angle of the triangular rod with respect to the x axis. (e) The lattice of the corresponding tight-binding model. (f) The reduced first Brillouin zone. For $\theta = 35°$, the bulk band structures at $(k_x, k_y) = (0, 4\pi/3a)$ (g) along the k_z direction and (h) in the k_x-k_y plane with $k_z = 0.57(\pi/h)$. The colored maps denote the magnitude of experimental Fourier spectra. There exists a minimal number of four ideal type-II WPs with positions shown in (f). The purple and green circles represent the WPs with charges $+1$ and -1, respectively.

found that the linear dispersion of the crossing point possesses group velocities in the same direction. And the linear dispersion appears at the $\bar{K}$ point, but the group velocities are in the opposite directions for the band structure in the k_x-k_y plane with $k_z = 0.57\pi/h$, as shown in Fig. 1(h). So the crossing point is a type-II WP with position at $(k_x, k_y, k_z) = [0, (4\pi/3a), 0.57(\pi/h)]$. The other three type-II WPs can be obtained by the symmetry. Figure 1(f) shows the minimal number of four type-II WPs in the first Brillouin zone with green and purple spheres denoting opposite charges. Time-reversal symmetry protects the WPs situated at the $\bar{K}$ and $\bar{K}'$ points having opposite charges, and mirror symmetry of the $z = 0$ plane protects the WPs situated at opposite k_z also having opposite charges. In addition, owing to the D_{3h} symmetry, the WPs are usually located along KH and $K'H'$ lines, making the WPs more easily searching. Therefore, these type-II WPs are ideal because of all of them being at the same frequency, guaranteed by time-reversal symmetry and mirror symmetry.

To study the evolution of these type-II WPs in our PCs, we calculate the bulk band structures at $(k_x, k_y) = [0, (4\pi/3a)]$ as functions of k_z and θ, as plotted in Fig. 2(a). When θ is in the range of $29.1° < \theta < 39°$, type-II WPs emerge as marked by the black dashed line. When $\theta < 29.1°$, the WPs eliminate at $k_z = 0$ and turn to open a bulk gap, while when $\theta > 39°$ the WPs eliminate at $k_z = \pm\pi/h$ and also open a bulk gap. The gaps for $\theta < 29.1°$ and $\theta > 39°$ should have different topological phases because of the separation of them being the WPs. So there are three topologically distinct phases I, II, and III, colored by gray, blue, and yellow in Fig. 2(b). Because of the D_{3h} symmetry, the band structure as a function of θ satisfies the periodicity of 120°. As the system has the mirror symmetry of the $y = 0$ plane at $\theta = 0°$, the topological phase for $\theta < 0°$ stays the same as that for its positive counterpart, thus only the topological phase for $0° < \theta < 60°$ is shown in Fig. 2. The topological properties of this system can be described by the k_z-dependent valley Chern number $C_V(k_z)$, as discussed from Eq. (3). Phases I and III are the distinct valley insulators, in which $C_V(k_z)$ along the KH line are $\frac{1}{2}$ and $-\frac{1}{2}$, respectively. Phase II is the Weyl semimetal, in which the WP along the KH line with $k_z > 0$ hosts the topological charge $C = \frac{1}{2} - (-\frac{1}{2}) = 1$ [purple dashed line in Fig. 2(b)], while the topological charge of the WP at opposite k_z is -1 (green dashed line). The region of the Weyl phase can be tuned by varying the two interlayer couplings or, in fact, the sizes of the two cutting-through holes with radii r_1 and r_2 [64]. These results are consistent with those of the analytic model.

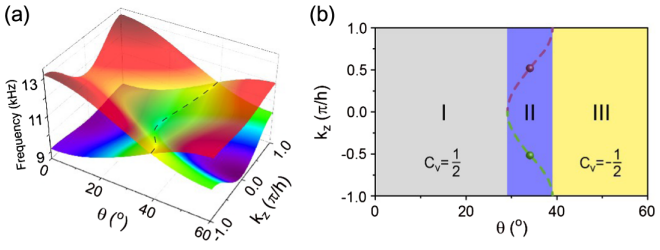

FIG. 2. (a) 3D band structures as functions of k_z and rotation angle θ at $(k_x, k_y) = [0, (4\pi/3a)]$. The dashed line outlines the WPs where the band gap closes. (b) The phase diagram determined by the k_z-dependent valley Chern numbers for θ. Phases I and III are topologically distinct valley insulators, while phase II is Weyl semimetal. The purple and green dashed lines in phase II represent the positions of WPs with opposite charges.

Weyl semimetal was predicted to give rise to the Fermi-arc surface states. Figure 3 shows the Fermi arcs of the states at $f = 10$ kHz on the left and right zigzag surfaces of the PC with $\theta = 35°$. The colored maps and lines represent the measured and simulated data, which are consistent with each other. For the full surface wave dispersions, one can refer to the Supplemental Material [64]. Interestingly, the Fermi arcs could connect the upper and lower WPs, or the left and right ones with opposite charges, relying on the surface structures. However, there are no Fermi arcs at the armchair surfaces, due to the cancellation of the projected WPs with opposite charges at the same k_z.

We then study the surface states on the interface between the two topologically distinct valley insulators, phases I and III, in which the valley Chern numbers along the KH line are $C_V(k_z) = \frac{1}{2}$ (phase I) and $-\frac{1}{2}$ (phase III), respectively. The valley insulator here can be viewed as the two-dimensional valley insulator [65–68] stacked to three dimensions, and is thus of weak topology [63,70]. Because of the k_z-dependent valley Chern number, the surface states exist at the interfaces (100) or (010), but not (001), of the two topologically distinct valley insulators [64]. The closed Fermi circles are different from the nonclosed Fermi arcs connecting the projections of the WPs with opposite charges. Figure 4(a) shows the calculated and measured Fermi-circle surface dispersions at

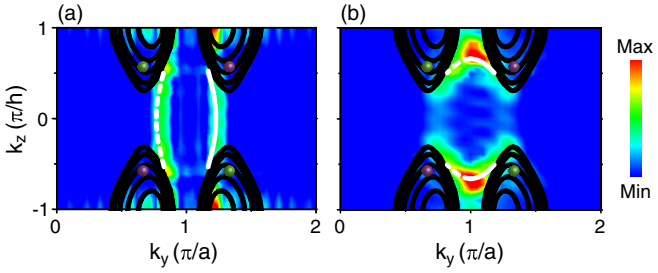

FIG. 3. The equifrequency contours at $f = 10$ kHz on the (a) left and (b) right zigzag surfaces of the PC with $\theta = 35°$ (phase II). The colored maps represent the measured data, and the black lines denote the calculated projected bulk states. The white dashed and solid lines denote the surface states projected from the V' and V valleys. The Fermi arcs could connect the upper and lower WPs, or the left and right ones, depending on the surface potentials.

$f = 10.7$ kHz for interface (100) formed by the two distinct valley insulators, with good agreement.

Unlike the Fermi-arc surface states that merge with the bulk states at the ends of the arcs, the Fermi-circle surface states can exist independently in the complete bulk gap and thus have particular advantage in surface transport. They can be excited without disturbing the bulk states. As a concrete example, we display an interesting wave partition of the surface states at the intersection channels. Figure 4(d) shows the schematic of the system constructed by four domains with channels 1–4, where the angle between channels 2 and 3 is 60°. The top left and bottom right domains (gray regions) belong to phase I with $\theta = 20°$, and the other two domains (yellow regions) are of phase III with $\theta = 50°$. A point source is placed at the position marked by a pink star at the left of channel 1 to excite the surface waves. Figure 4(e) shows the corresponding sample. The simulated and measured field distributions of wave partition are shown in Figs. 4(f) and 4(g) with good agreement. The directions of group velocities in channels 1, 2, and 4 are shown in Figs. 4(a)–4(c). The incident waves from channel 1 only enter into channels 2 and 4 with the positive group velocities, because of the valley-momentum locking. Dramatically, the sound waves mainly propagate to channel 4 with a sharp turn, since the surface states near a sharp turn can be coupled more easily, similar to the partition of the edge states in the two-dimensional topological system [71–73]. The surface waves also split into two parts along the z direction, coming from the specific surface wave dispersions shown in Figs. 4(a)–4(c).

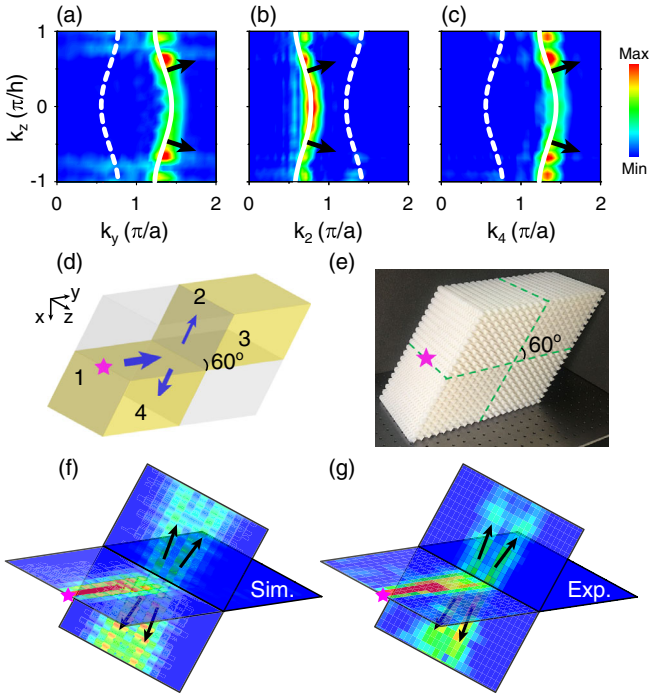

FIG. 4. (a)–(c) The equifrequency contours at $f = 10.7$ kHz for the interfaces 1, 2, 4 in (d) formed by the PCs with $\theta = 20°$ (phase I, gray region) and $\theta = 50°$ (phase III, yellow region). The k_2 and k_4 denote the wave vectors along the directions of interfaces 2 and 4 marked by blue arrows in (d). The experimental results are obtained by the Fourier transformation of the field distributions in (g), where only the states with positive group velocities (black arrows) are excited. (d) Schematic of the wave partition at an intersection with channels (interfaces) 1–4, where the angle between channels 2 and 3 is 60°. The incident waves from channel 1 are forbidden to channel 3 and tend to propagate to channel 4 with a sharp turn (shown by the size of blue arrows). (e) A photo of the corresponding sample. (f),(g) The simulated and measured field distributions excited by a point source (pink star) from channel 1 at $f = 10.7$ kHz.

In conclusion, we have realized an ideal type-II Weyl phase and observed the topological phase transition to valley insulators. Our system not only provides special advantages to explore the intriguing properties of type-II Weyl semimetals, but also paves a potential way for applications of topological acoustics. For example, the topological transport and wave partition of the surface states may serve as a basis for acoustic devices, such as waveguide, splitter, and signal processing in a network structure. Moreover, the acoustic vortex property induced by the valley nature [74] may make our system as 3D acoustic tweezers and rotate the trapped microparticles in the absence of contact.

This work is supported by the National Key R&D Program of China (Grant No. 2018YFA0305800), the National Natural Science Foundation of China (Grants No. 11804101, No. 11890701, No. 11704128, No. 11774275, No. 11974120, No. 11974005), the Guangdong Innovative and Entrepreneurial Research Team Program (Grant No. 2016ZT06C594), the Guangdong Basic and Applied Basic Research Foundation (Grant No. 2019B151502012), and the Fundamental Research Funds for the Central Universities (Grants No. 2018MS93, No. 2019JQ07, No. 2019ZD49).

Note added.—Recently, we become aware of a preprint [75] that focuses on the ideal type-II Weyl points in electric circuit.

*Corresponding author.
dengwy@scut.edu.cn
†Corresponding author.
phjylu@scut.edu.cn
‡Corresponding author.
zyliu@whu.edu.cn

[1] B. A. Bernevig, Nat. Phys. **11**, 698 (2015).
[2] N. P. Armitage, E. J. Mele, and A. Vishwanath, Rev. Mod. Phys. **90**, 015001 (2018).
[3] X. Wan, A. M. Turner, A. Vishwanath, and S. Y. Savrasov, Phys. Rev. B **83**, 205101 (2011).
[4] A. A. Burkov and L. Balents, Phys. Rev. Lett. **107**, 127205 (2011).

[5] G. Xu, H. Weng, Z. Wang, X. Dai, and Z. Fang, Phys. Rev. Lett. **107**, 186806 (2011).
[6] K. Y. Yang, Y. M. Lu, and Y. Ran, Phys. Rev. B **84**, 075129 (2011).
[7] H. Weng, C. Fang, Z. Fang, B. A. Bernevig, and X. Dai, Phys. Rev. X **5**, 011029 (2015).
[8] S. M. Huang *et al.*, Nat. Commun. **6**, 7373 (2015).
[9] L. Wang, S. K. Jian, and H. Yao, Phys. Rev. A **93**, 061801 (R) (2016).
[10] A. C. Potter, I. Kimchi, and A. Vishwanath, Nat. Commun. **5**, 5161 (2014).
[11] D. T. Son and B. Z. Spivak, Phys. Rev. B **88**, 104412 (2013).
[12] A. A. Burkov, Phys. Rev. B **91**, 245157 (2015).
[13] M. X. Deng, G. Y. Qi, R. Ma, R. Shen, R. Q. Wang, L. Sheng, and D. Y. Xing, Phys. Rev. Lett. **122**, 036601 (2019).
[14] X. Huang, L. Zhao, Y. Long, P. Wang, D. Chen, Z. Yang, and H. Liang, Phys. Rev. X **5**, 031023 (2015).
[15] C. L. Zhang *et al.*, Nat. Commun. **7**, 10735 (2016).
[16] J. Liu and D. Vanderbilt, Phys. Rev. B **90**, 155316 (2014).
[17] A. A. Soluyanov, D. Gresch, Z. Wang, Q. Wu, M. Troyer, X. Dai, and B. A. Bernevig, Nature (London) **527**, 495 (2015).
[18] Y. Xu, F. Zhang, and C. Zhang, Phys. Rev. Lett. **115**, 265304 (2015).
[19] Z. Wang, D. Gresch, A. A. Soluyanov, W. Xie, S. Kushwaha, X. Dai, M. Troyer, R. J. Cava, and B. A. Bernevig, Phys. Rev. Lett. **117**, 056805 (2016).
[20] A. Tamai *et al.*, Phys. Rev. X **6**, 031021 (2016).
[21] G. Chang *et al.*, Sci. Adv. **2**, e1600295 (2016).
[22] M. Udagawa and E. J. Bergholtz, Phys. Rev. Lett. **117**, 086401 (2016).
[23] Y. Y. Lv *et al.*, Phys. Rev. Lett. **118**, 096603 (2017).
[24] Z. M. Yu, Y. Yao, and S. A. Yang, Phys. Rev. Lett. **117**, 077202 (2016).
[25] S. Y. Xu *et al.*, Science **349**, 613 (2015).
[26] B. Q. Lv *et al.*, Phys. Rev. X **5**, 031013 (2015).
[27] L. X. Yang, Z. K. Liu, Y. Sun, H. Peng, H. F. Yang, T. Zhang, B. Zhou, Y. Zhang, Y. F. Guo, M. Rahn, D. Prabhakaran, Z. Hussain, S.-K. Mo, C. Felser, B. Yan, and Y. L. Chen, Nat. Phys. **11**, 728 (2015).
[28] B. Q. Lv *et al.*, Nat. Phys. **11**, 724 (2015).
[29] K. Deng *et al.*, Nat. Phys. **12**, 1105 (2016).
[30] L. Huang, T. M. McCormick, M. Ochi, Z. Zhao, M. T. Suzuki, R. Arita, Y. Wu, D. Mou, H. Cao, J. Yan, N. Trivedi, and A. Kaminski, Nat. Mater. **15**, 1155 (2016).
[31] J. Jiang *et al.*, Nat. Commun. **8**, 13973 (2017).
[32] M.-Y. Yao, N. Xu, Q. S. Wu, G. Autes, N. Kumar, V. N. Strocov, N. C. Plumb, M. Radovic, O. V. Yazyev, C. Felser, J. Mesot, and M. Shi, Phys. Rev. Lett. **122**, 176402 (2019).
[33] L. Lu, L. Fu, J. D. Joannopoulos, and M. Soljacic, Nat. Photonics **7**, 294 (2013).
[34] L. Lu, Z. Wang, D. Ye, L. Ran, L. Fu, J. D. Joannopoulos, and M. Soljacic, Science **349**, 622 (2015).
[35] W. J. Chen, M. Xiao, and C. T. Chan, Nat. Commun. **7**, 13038 (2016).
[36] B. Yang, Q. Guo, B. Tremain, L. E. Barr, W. Gao, H. Liu, B. Béri, Y. Xiang, D. Fan, A. P. Hibbins, and S. Zhang, Nat. Commun. **8**, 97 (2017).
[37] J. Noh, S. Huang, D. Leykam, Y. D. Chong, K. P. Chen, and M. C. Rechtsman, Nat. Phys. **13**, 611 (2017).
[38] M. Xiao, W. J. Chen, W. Y. He, and C. T. Chan, Nat. Phys. **11**, 920 (2015).
[39] Z. Yang and B. Zhang, Phys. Rev. Lett. **117**, 224301 (2016).
[40] F. Li, X. Huang, J. Lu, J. Ma, and Z. Liu, Nat. Phys. **14**, 30 (2018).
[41] H. He, C. Qiu, L. Ye, X. Cai, X. Fan, M. Ke, F. Zhang, and Z. Liu, Nature (London) **560**, 61 (2018).
[42] H. Ge, X. Ni, Y. Tian, S. K. Gupta, M. H. Lu, X. Lin, W. D. Huang, C. T. Chan, and Y. F. Chen, Phys. Rev. Applied **10**, 014017 (2018).
[43] T. G. Chen, J. R. Jiao, H. Q. Dai, and D. J. Yu, Phys. Rev. B **98**, 214110 (2018).
[44] B. Xie, H. Liu, H. Cheng, Z. Liu, S. Chen, and J. Tian, Phys. Rev. Lett. **122**, 104302 (2019).
[45] J. Ruan, S. K. Jian, H. Yao, H. Zhang, S. C. Zhang, and D. Xing, Nat. Commun. **7**, 11136 (2016).
[46] J. Ruan, S. K. Jian, D. Zhang, H. Yao, H. Zhang, S. C. Zhang, and D. Xing, Phys. Rev. Lett. **116**, 226801 (2016).
[47] G. Autès, D. Gresch, M. Troyer, A. A. Soluyanov, and O. V. Yazyev, Phys. Rev. Lett. **117**, 066402 (2016).
[48] G. Chang, S.-Y. Xu, D. S. Sanchez, S.-M. Huang, C.-C. Lee, T.-R. Chang, G. Bian, H. Zheng, I. Belopolski, N. Alidoust, H.-T. Jeng, A. Bansil, H. Lin, and M. Z. Hasan, Sci. Adv. **2**, e1600295 (2016).
[49] B. W. Xia, R. Wang, Z. J. Chen, Y. J. Zhao, and H. Xu, Phys. Rev. Lett. **123**, 065501 (2019).
[50] J. Liu, W. Hou, E. Wang, S. Zhang, J.-T. Sun, and S. Meng, Phys. Rev. B **100**, 081204(R) (2019).
[51] B. Yang, Q. Guo, B. Tremain, R. J. Liu, L. E. Barr, Q. Yan, W. Gao, H. Liu, Y. Xiang, J. Chen, C. Fang, A. Hibbins, L. Lu, and S. Zhang, Science **359**, 1013 (2018).
[52] J. Lu, C. Qiu, L. Ye, X. Fan, M. Ke, F. Zhang, and Z. Liu, Nat. Phys. **13**, 369 (2017).
[53] J. Lu, C. Qiu, W. Deng, X. Huang, F. Li, F. Zhang, S. Chen, and Z. Liu, Phys. Rev. Lett. **120**, 116802 (2018).
[54] Y. Ding, Y. Peng, Y. Zhu, X. Fan, J. Yang, B. Liang, X. Zhu, X. Wan, and J. Cheng, Phys. Rev. Lett. **122**, 014302 (2019).
[55] X. Zhang, H.-X. Wang, Z.-K. Lin, Y. Tian, B. Xie, M.-H. Lu, Y.-F. Chen, and J.-H. Jiang, Nat. Phys. **15**, 582 (2019).
[56] X. Ni, M. Weiner, A. Alu, and A. B. Khanikaev, Nat. Mater. **18**, 113 (2019).
[57] H. Xue, Y. Yang, F. Gao, Y. Chong, and B. Zhang, Nat. Mater. **18**, 108 (2019).
[58] C. He, S.-Y. Yu, H. Wang, H. Ge, J. Ruan, H. Zhang, M.-H. Lu, and Y.-F. Chen, Phys. Rev. Lett. **123**, 195503 (2019).
[59] V. Peri, Z.-D. Song, M. Serra-Garcia, P. Engeler, R. Queiroz, X. Huang, W. Deng, Z. Liu, B. A. Bernevig, and S. D. Huber, Science **367**, 797 (2020).
[60] V. Peri, M. Serra-Garcia, R. Ilan, and S. D. Huber, Nat. Phys. **15**, 357 (2019).
[61] C. He, S. Y. Yu, H. Ge, H. Wang, Y. Tian, H. Zhang, X. C. Sun, Y. B. Chen, J. Zhou, M. H. Lu, and Y. F. Chen, Nat. Commun. **9**, 4555 (2018).
[62] W. Deng, J. Lu, F. Li, X. Huang, M. Yan, J. Ma, and Z. Liu, Nat. Commun. **10**, 1769 (2019).
[63] M. Z. Hasan and C. L. Kane, Rev. Mod. Phys. **82**, 3045 (2010).
[64] See Supplemental Material at http://link.aps.org/supplemental/10.1103/PhysRevLett.124.206802 for more details on the theoretical model, phase diagram, and the

calculated results about the extension of the surface and interface states.
[65] D. Xiao, W. Yao, and Q. Niu, Phys. Rev. Lett. **99**, 236809 (2007).
[66] G. W. Semenoff, V. Semenoff, and F. Zhou, Phys. Rev. Lett. **101**, 087204 (2008).
[67] I. Martin, Y. M. Blanter, and A. F. Morpurgo, Phys. Rev. Lett. **100**, 036804 (2008).
[68] F. Zhang, J. Jung, G. A. Fiete, Q. Niu, and A. H. MacDonald, Phys. Rev. Lett. **106**, 156801 (2011).
[69] F. Zhang, A. H. MacDonald, and E. J. Mele, Proc. Natl. Acad. Sci. U.S.A. **110**, 10546 (2013).
[70] R. Noguchi *et al.*, Nature (London) **566**, 518 (2019).
[71] Z. Qiao, J. Jung, C. Lin, Y. Ren, A. H. MacDonald, and Q. Niu, Phys. Rev. Lett. **112**, 206601 (2014).
[72] M. Yan, J. Lu, F. Li, W. Deng, X. Huang, J. Ma, and Z. Liu, Nat. Mater. **17**, 993 (2018).
[73] Z. Zhu, X. Huang, J. Lu, M. Yan, F. Li, W. Deng, and Z. Liu, Phys. Rev. Applied **12**, 024007 (2019).
[74] J. Lu, C. Qiu, M. Ke, and Z. Liu, Phys. Rev. Lett. **116**, 093901 (2016).
[75] R. Li, B. Lv, H. Tao, J. Shi, Y. Chong, B. Zhang, and H. Chen, arXiv:1910.03503.